

Mobility of antifreeze proteins as a key factor in their use to control ice growth on surfaces and polymers

Hoebus, Laura; Tavaststjerna, Miisa J.; Garcia, Santiago J.

DOI

[10.1016/j.apsadv.2025.100790](https://doi.org/10.1016/j.apsadv.2025.100790)

Publication date

2025

Document Version

Final published version

Published in

Applied Surface Science Advances

Citation (APA)

Hoebus, L., Tavaststjerna, M. J., & Garcia, S. J. (2025). Mobility of antifreeze proteins as a key factor in their use to control ice growth on surfaces and polymers. *Applied Surface Science Advances*, 28, Article 100790. <https://doi.org/10.1016/j.apsadv.2025.100790>

Important note

To cite this publication, please use the final published version (if applicable). Please check the document version above.

Copyright

Other than for strictly personal use, it is not permitted to download, forward or distribute the text or part of it, without the consent of the author(s) and/or copyright holder(s), unless the work is under an open content license such as Creative Commons.

Takedown policy

Please contact us and provide details if you believe this document breaches copyrights. We will remove access to the work immediately and investigate your claim.



Full Length Article

Mobility of antifreeze proteins as a key factor in their use to control ice growth on surfaces and polymers

Laura Hoebus , Miisa J. Tavaststjerna , Santiago J. Garcia 

Department of Aerospace Structures and Materials, Faculty of Aerospace Engineering, Delft University of Technology, Kluyverweg 1, 2629 HS, Delft, The Netherlands



ARTICLE INFO

Keywords:

Anti-icing
Ice-binding proteins
Anti-freeze proteins
Ice adhesion
Bioinspired
Functional coatings

ABSTRACT

The successful use of ice-binding proteins (IBPs) to develop anti-icing surfaces requires a comprehensive understanding of their working mechanism when introduced in environments distinct from the protein's natural setting. This study systematically addresses this aspect by investigating how IBPs control ice accretion when grafted onto an aluminum alloy using polyethylene glycol (PEG) linkers of various lengths and on the polymer backbone of a PEG hydrogel matrix. Freezing experiments monitored through thermal imaging reveal that the degrees of freedom of the proteins significantly influence their functionality. Specifically, we demonstrate that when the degrees of freedom of anti-freeze proteins (AFPs) are restricted by their functionalization on surfaces using short linkers or when they are present in restricted volumes in polymers, they behave as ice-nucleating proteins (INPs) promoting ice accretion. In conditions where their degrees of freedom are enhanced (long linkers, water-rich environment), AFPs effectively inhibit ice nucleation and propagation. The work underlines the relevance of protein mobility as a so far unforeseen key design factor needed to fully benefit from the potential use of natural or synthetic AFPs grafted on surfaces for cryopreservation of biological samples and the design of next-generation low-icing surfaces and coatings.

1. Introduction

In cold climates, the formation and accumulation of ice on surfaces can instigate safety hazards and damage in a wide range of applications such as building roofs [1], power lines [2,3], wind turbines [3,4], and aircraft [5,6]. For example, ice accumulation on solar panels decreases their efficiency while ice on aircraft wings and tail can disrupt the airflow leading to a decrease in aircraft speed and lift, an increase in fuel consumption, and an overall decrease in safety during flight [1,6]. Moreover, low ice surfaces are of large relevance in the cryopreservation of biological materials and food, where the challenge of manufacturing high-yield cryoprotectants remains [7,8].

As in many other naturally occurring phenomena, natural evolution has provided solutions for successfully controlling ice formation and growth that can be used as inspiration to develop anti-icing surfaces. To increase the survival potential of species as diverse as plants, algae, fish, or insects, nature mostly relies on the production of a variety of proteins with the ability to interfere with ice crystal growth known as ice-binding proteins (IBPs). IBPs can be grouped in two major classes depending on their principal strategy used to protect the species against freezing: (i)

ice-nucleating proteins (INPs) which accelerate ice formation, and (ii) anti-freeze proteins (AFPs) which delay ice formation [9,10].

Most of the available literature focuses on the role of the natural or synthetic IBP chemistry on ice control in fluids [7,11–13], while only a few groups reported on the use of AFPs on surfaces to induce passive anti-icing behavior [14–18]. One of the major challenges in the use of AFPs on surfaces appears to be the apparently unexplained discrepancy in results regarding the positive or negative effect of AFPs on surfaces. For example, AFPs from *Chaetoceros neogratic* (an Antarctic marine diatom) immobilized on an aluminum surface using an Al-binding peptide delayed ice formation for three hours in an air-cold chamber at $-3.5\text{ }^{\circ}\text{C}$ and 84 % relative humidity [14]. Similarly, type III AFP from *Zoarces americanus* (a polar fish), grafted onto a polymer backbone covalently bound to an aldehyde-coated glass slide showed a freezing delay from 20 min without AFP to 45 min with AFP at $-6\text{ }^{\circ}\text{C}$ and 40 % RH [15]. Contrary to these results, the same type III AFP on aluminum showed that AFPs promoted earlier ice nucleation instead of inhibiting it when the surfaces were cooled at $-0.5\text{ }^{\circ}\text{C min}^{-1}$ until ice nucleation occurred [16]. Part of the apparently contradicting results in literature can be attributed to the use of very different manufacturing techniques,

* Corresponding author.

E-mail address: s.j.garciaespallargas@tudelft.nl (S.J. Garcia).

process conditions, freezing tests, and AFPs. Nevertheless, besides chemistry, other more fundamental AFP architectural factors may also play a relevant role in IBP behavior used in synthetic materials. For instance, while in nature ice growth inhibition induced by AFPs increases with increasing AFP concentration in solution [19], no systematic studies on the effect of protein concentration on surfaces have been reported. Similarly, a study using AFPs from *Microdera punctipennis dzungarica* (an insect) suggests that the protein orientation relative to the surface may play an important role in ice nucleation [20]. With some reports showcasing the beneficial effects of AFPs and some their negative effects and the myriad of factors affecting behavior of different proteins, more mechanistic understanding on the factors leading to a positive or a negative effect with the same protein appears as a necessary step to understand discrepancies and boost research and applications of AFP for ice-controlling surfaces.

In this work, we discuss the key role that the degrees of freedom (mobility) of grafted proteins has on surface ice nucleation and growth. To this aim, two model IBPs (an AFP type III from fish and an INP from bacteria) were grafted at varying concentrations and linker chain lengths on (i) aluminum substrates and (ii) as dangling chains in the polymer backbone of a model hydrogel. This strategy allowed us to study the effect of mobility on ice formation using the same protein type in a well-controlled fashion. The work outlines the behavioral similarities between the studied AFPs and INPs and the relevance of protein mobility and surface water layers for effective anti-freezing. Not disregarding protein chemistry diversity, the work underpins the importance of protein degrees of freedom as a design rule to develop future anti-freezing surfaces and coatings using natural and synthetic proteins and molecules with comparable structures and mechanisms.

2. Materials and methods

2.1. Materials

Two model ice-binding proteins (IBPs) were used in this work selected based on size, functionality, information, and availability: (i) type III AFP from *Marcrozoarces americanus* fish (6.5 kDa, ~2.5 nm coiled diameter), obtained from A/F Protein Inc.; and (ii) INPs from *Pseudomonas syringae* bacteria (~100 kDa, ~10 nm coiled diameter) purchased from Snomax Inc. 3-mercaptopropyltrimethoxysilane (MPTS, 96 %) was bought from Gelest Inc.. Sodium hydroxide pellets (anhydrous NaOH, ≥ 98 %), phosphate-buffered saline (PBS, pH 7.4) solution, 4arm-PEG-maleimide (average $M_n = 10$ kDa), PEG dithiol (average $M_n = 1$ kDa), and three maleimide-PEG-succinimidyl ester linker with three different repeating units of PEG (2, 12, 24) (Mal-PEG_{2/12/24}-NHS) were bought from Sigma-Aldrich. All solvents were of technical grade and used as received.

2.2. Preparation of IBP-grafted aluminum alloy surfaces

2.2.1. Aluminum alloy surface preparation

AA2024-T3 samples (2 cm x 2 cm x 3 mm) were manually and sequentially ground with 18 μm, 10 μm, and 6 μm grain size grinding paper. Between each grinding step, the samples were placed in an ultrasonic ethanol bath for 2 min. After grinding, the samples were sequentially polished with 3 μm and 0.25 μm particle size diamond paste reaching a surface roughness $S_a \approx 0.104$ μm. Finally, to remove any remaining contaminants, the samples were rinsed with acetone prior to subsequent surface treatment steps.

2.2.2. Surface functionalization of aluminum alloy substrates

Surface activation of AA2024-T3 was obtained by submerging the polished samples in a 2 M NaOH solution for 10 s, rinsed with deionized (DI) water, and dried in an oven at 100 °C for 30 min to remove any excess water. The samples obtained with this process are further named “AA2024-OH”. The resulting hydroxyl-rich pseudoboehmite layer was

subsequently used for surface modification through silanization to obtain thiol-rich surfaces (samples named “AA2024-SH”). Silanization was obtained by immersing the metal plates in a 2:30 water:methanol mixture (96 ml) with 4 ml of 3-mercaptopropyltrimethoxysilane (MPTS) for 2 h. Before immersion, the silane solution was stirred for 24 h to ensure sufficient pre-hydrolysis of the MPTS. After 2 h immersion in the MPTS solution, the samples were rinsed with methanol, dried in a vacuum for 30 min, and cured in an oven for 1 hour at 100 °C.

2.2.3. Modification of the IBPs with PEG linkers of different lengths

An IBP solution (0.1 mM) was prepared by dissolving the dry protein powder in a phosphate-buffered saline solution (PBS, pH 7.4). Next, a stock solution with 250 mM PEG linker was prepared by mixing Mal-PEG_{2/12/24}-NHS with DMSO. The linker solution was then added to the IBP solution in tenfold molar excess (4 μl of linker stock solution per 1 ml of IBP solution). The mixture was stirred for 1 hour at a pH of 7.4 to ensure a complete and selective reaction between the protein amine end group and the linker succinimidyl ester group. Finally, to obtain Mal-PEG_{2/12/24}-NH-IBPs, the excess linker and side products were removed by centrifuging the mixture three times for 5 min at 4400 rpm. After each centrifuging step, the heavy Mal-PEG_{2/12/24}-NH-IBPs precipitate to the bottom. The supernatant is then pipetted out of the tube while fresh PBS is added to the precipitated Mal-PEG_{2/12/24}-NH-IBPs. Finally, Mal-PEG_{2/12/24}-NH-IBPs is stored in a PBS solution in a freezer at -20 °C.

2.2.4. Grafting of MAL-PEG_{2/12/24}-NH-IBPs on aluminum alloy substrate

The Mal-PEG_{2/12/24}-NH-IBPs are extracted from their PBS solution and various weights of Mal-PEG_{2/12/24}-NH-IBPs (2.5 mg and 5 mg) are redispersed in 1 ml PBS to obtain different IBP concentrations in solution. The AA2024-SH samples were then immersed in this protein solution for 4 h. During the process, the maleimide functionality from the modified IBPs reacts with thiol groups at the aluminum surface through thiol-Michael click chemistry, hence leading to aluminum surfaces grafted with IBPs with different linker lengths. After immersion, the IBP-modified AA2024 samples were rinsed with DI water and dried in a vacuum at room temperature overnight to remove any excess water.

2.3. Preparation of IBP-modified hydrogels on aluminum alloy surfaces

IBP-containing hydrogels of approximately 10 wt % were produced by preparing two separate solutions: (1) solution 1: PEG dithiol dispersed in 0.1 ml PBS at 6.5:100 (w/w) ratio; and (2) solution 2: 4arm-PEG-maleimide (average $M_n = 10\,000$ g mol⁻¹) in 0.1 ml PBS at 15.5:100 (w/w) ratio. To solution 2, 0 mg, 2.5 mg or 5 mg Mal-PEG₁₂-NH-IBPs was added to produce hydrogels with varying IBP concentrations. The final protein-hydrogel was produced by spraying with a lab-built Confined Impinging Jet (CIJ) mixer [21]. The PEG dithiol solution (solution 1) was added to one side of the CIJ mixer while the 4-arm PEG maleimide/ Mal-PEG₁₂-NH-IBP solution (solution 2) was inserted on the other side. Next, both openings of the mixer are connected to high-pressure inlets, thus spraying the two solutions simultaneously through an outlet point on the AA2024-SH substrate. By Thiol-Michael click chemistry between the thiol functionalities present in solution 1 and the maleimide functionalities from solution 2, a hydrogel with grafted proteins is developed.

2.4. Water contact angle (WCA) measurements

Static WCA measurements were performed with a Tensiometer KSV CAM 200 (KSV Instruments Ltd., Finland) as an indirect test to confirm surface modification of the alloys after surface activation and silanization. For each sample condition, three repeats using 5 μl DI water droplets were performed. Droplet shape analysis of the images was done to obtain the WCA of the surfaces. All WCA measurements were carried out at an ambient temperature of 21 °C ± 2 and relative humidity of 40

% ± 5 .

2.5. Raman spectroscopy

Raman spectroscopy measurements were performed on untreated, activated and silanized AA2024 samples to confirm successful chemical treatments. To this aim, a Renishaw inVia Raman microscope with a laser length of 532 nm was used. For each measurement point, 16 accumulations were made at 10 % laser power with an exposure time of 60 s.

2.6. Fourier transform infrared spectroscopy (FTIR)

FTIR was first used to monitor the reaction between the protein and PEG linker in solution by measuring the solutions at different points in time. FTIR was further used to confirm surface grafting with proteins. To this aim, a Spectrum 100 FTIR Spectrometer (Perkin Elmer) was used and run from 4000 to 500 cm^{-1} to obtain the FTIR spectra as the average of 32 scans.

2.7. Differential scanning calorimetry (DSC)

A DSC 250 (TA Instruments) was used to determine the state of water present in the hydrogel polymer networks (adsorbed and absorbed) following guidelines reported in recent works [22]. Hydrogel samples of 5 mg were placed in the DSC and tested for two cycles with the following cooling-heating protocol: sample equilibration at 20 °C for 5 min, cooling from 20 °C to -50 °C at a rate of -10 °C min^{-1} , isotherm at -50 °C for 5 min, heating to 20 °C at 10 °C min^{-1} . Three different samples were tested for each hydrogel composition for reproducibility.

2.8. Frosting tests monitored by thermal imaging

To monitor and quantify the freezing events of the samples, a homemade freezing set-up was used. Samples are placed on top of a liquid-

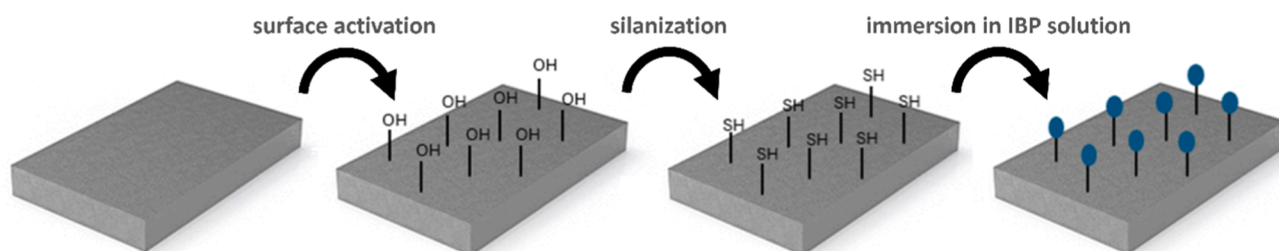
cooled plate (TECA LHP-300CP) which is powered by a 11.5 DC voltage source within a small isolating chamber to control well humidity (RH was set at 38 % ± 3 for all experiments) and temperature. This allowed cooling the samples at -10 °C min^{-1} until -20 °C. The freezing events and propagation were monitored using a FLIR A655sc thermal camera with a close-up lens (1.5 magnifying factor and 25 μm resolution). The surfaces are monitored with the thermal camera right after cooling starts, hence allowing a good image-freezing time correlation as reported elsewhere [23]. The recorded times and temperatures were directly plot in the FLIR tools program using a emissivity of 0.4 for the protein-modified surfaces (similar to emissivity of oxidized aluminum) and 0.9 for the hydrogels. From the plots the freezing onset time (t_{fo}) was obtained as the time until surface freezing was observed and the freezing onset temperature (T_{fo}), as the temperature on the graph at which the freezing event starts (observed as temperature rise).

3. Results and discussion

3.1. Aluminum surface functionalization with IBPs

Fig. 1a shows the steps used to functionalize the aluminum surfaces with IBPs. This process consists of several steps using click chemistry explained in the experimental section: (i) activation, leading to hydroxyl-rich surfaces (AA2024-OH); (ii) silanization to enrich the surface with thiol groups (AA2024-SH), and; (iii) functionalization with INP or AFP (IBP) using maleimide-PEG oligomers [16]. This step-wise process provided surfaces with different proteins (AFP or INP), chain lengths (2, 12 or 24 PEG chains) and concentration (given by the protein concentration present in solution) as shown in Table 1. To achieve functionalization with IBPs, the IBPs were modified with a Mal-PEG_{2/12/24}-NHS linker where the succinimidyl ester (-NHS) selectively reacts with the IBP amine group at its N-terminus, forming an amide group and leading to the oligomers named as Mal-PEG_{2/12/24}-NH-IBP, where IBP can be AFP or INP (Fig. 1b showing the reaction steps). To separate the Mal-PEG_{2/12/24}-NH-IBPs from the byproduct, the samples

a) IBP surface development



b) IBP solution preparation

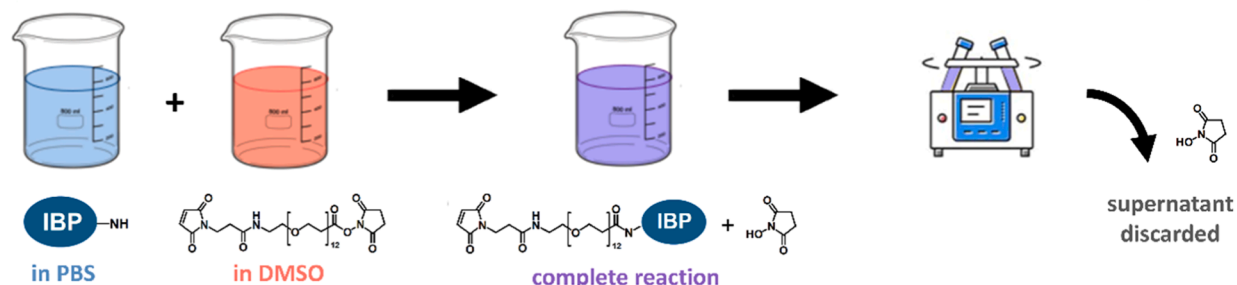


Fig. 1. a) Step-wise process to functionalize the aluminum surfaces leading to samples rich in -OH, -SH and -IBP; b) Chemical scheme to obtain functionalized IBPs (Mal-PEG_{2/12/24}-NH-IBP, in purple) from the reaction between NH₂-rich IBP (blue) and Mal-PEG_{2/12/24}-NHS oligomer (orange). The maleimide-functionality (Mal) allows grafting the extended IBPs onto the -SH rich aluminum surfaces via click-chemistry.

Table 1

Mal-PEG_{2/12/24}-NH-IBP solutions with varying protein type (AFP or INP), PEG linker length and protein concentration, used to graft IBPs on the AA2024-SH surfaces.

Characteristic parameters	Mal-PEG _{2/12/24} -NH-IBP solutions in PBS					
Solution no.	1	2	3	4	5	6
Type of protein	AFP	AFP	AFP	AFP	INP	INP
PEG linker length (number of repeating units)	12	12	2	24	12	12
Protein concentration (mg ml ⁻¹)	2.5	5.0	2.5	2.5	2.5	5.0

were centrifuged, the surplus liquid with byproduct removed, and the solid product redispersed in PBS forming a Mal-PEG_{2/12/24}-NH-IBPs solution. Finally, the AA2024-SH surfaces were immersed in the Mal-PEG_{2/12/24}-NH-IBP solutions to obtain surfaces grafted with different IBPs, PEG chain-length and IBP surface concentration. Since the ice-binding site (IBS) and the end groups of type III AFP are located on the opposite sides of the globular protein, this grafting approach targeting the N-terminus ensures that the IBS of the type III AFP will be

exposed after the surface functionalization.

Static WCA measurements and Raman spectroscopy were used to verify the chemical surface changes induced by activation and silanization, as shown in Fig. 2a,b. After immersion in NaOH, the static WCA decreases from 80° to 36° (Fig. 2a) as expected for a surface richer in pseudoboehmite structure containing hydroxyl groups. The surface modification is confirmed by Raman spectroscopy (Fig. 2b) revealing the appearance of peaks related to pseudoboehmite [24]: (i) 3000–3600 cm⁻¹ and 1650 cm⁻¹ attributed to -OH stretching and deformation vibrations of weakly bound water and (ii) a peak at 1050 cm⁻¹ corresponding to Al-O bending vibrations.

After silanization of AA2024-OH with MPTS thiol-terminated silane, the static WCA increases from 36° to 65° (Fig. 2a). This increase in WCA can be explained by the relatively lower hydrophilicity of thiol groups compared to hydroxyl groups. Raman analysis further confirmed the presence of silanes, and consequently thiols, on the surface: two peaks centered around 970 cm⁻¹ and 1050 cm⁻¹ corresponding to Si-O-Si stretching vibrations, one prominent peak at around 2950 cm⁻¹ characteristic for C-H stretching, and a peak around 1450 cm⁻¹ associated to the bending vibration of the -CH₂ group [25–27].

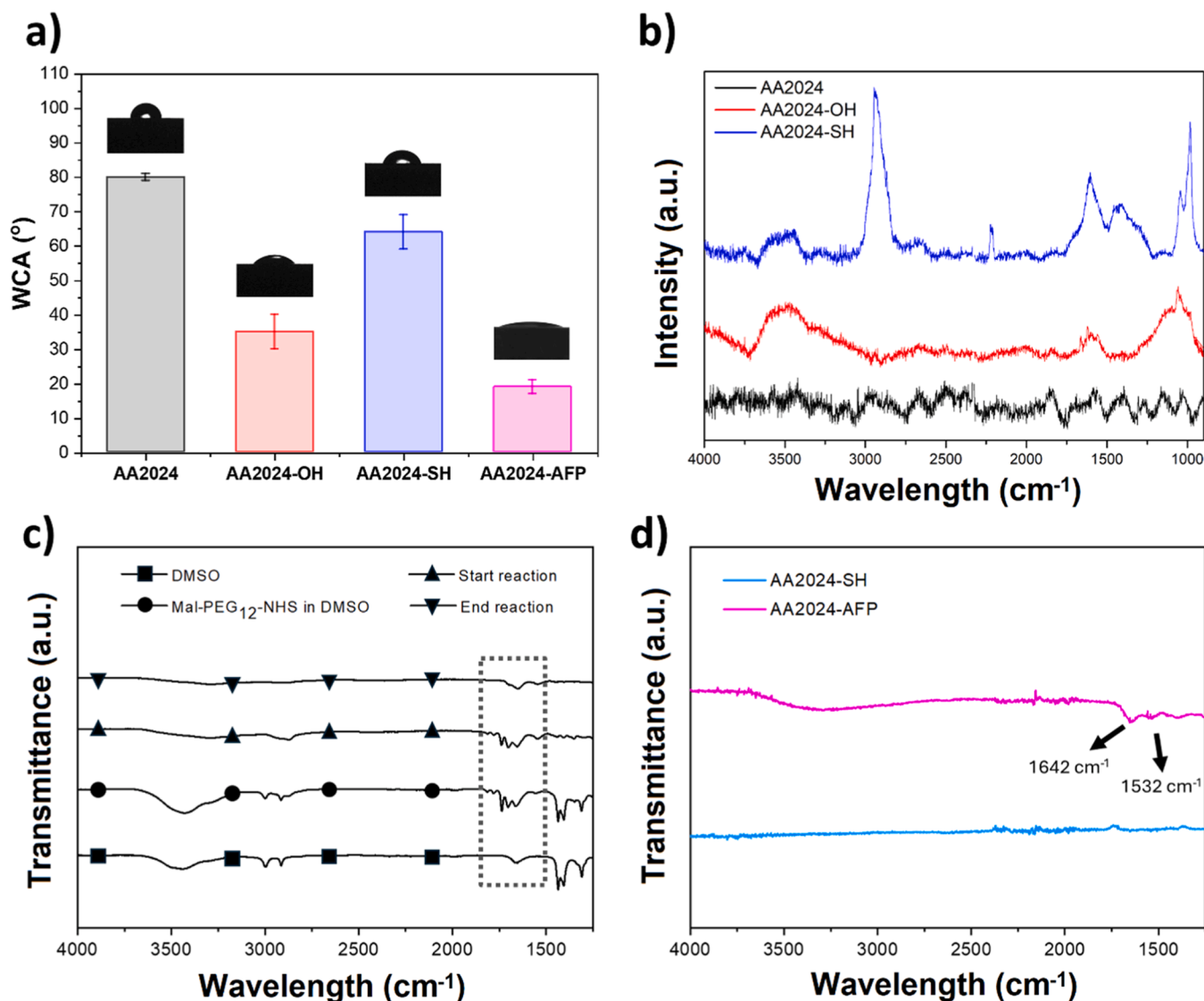


Fig. 2. a) Static water contact angle (WCA) and b) Raman spectra of polished AA2024 (black color), AA2024-OH (red color), and AA2024-SH (blue color); c) FTIR spectra of DMSO (squares), Mal-PEG₁₂-NHS in DMSO as a solvent (circles), start of the IBP/Mal-PEG₁₂-NHS reaction (triangles up), and end of the reaction (triangles down). d) FTIR spectra of AA2024-SH surface (blue) and AA2024-AFP surface (magenta) after immersion in IBP solution 1. The arrows mark the peaks of interest to confirm the reaction and surface modification.

To verify the reaction between the IBPs and the Mal-PEG_{2/12/24}-NHS linkers in solution, FTIR measurements were taken before, at the start, and at the end of the reaction. As seen in Fig. 2c, most of the peaks in the Mal-PEG₁₂-NHS in DMSO spectrum (circles) can be attributed to the DMSO solvent itself (squares). Nevertheless, one distinct peak at 1741 cm⁻¹ is associated with C = O stretching vibration of the succinimidyl ester from Mal-PEG₁₂-NHS and can be used to monitor the reaction with the protein (see the squared region in Fig. 2c). When IBPs are added to the solution, the peaks related to the succinimidyl are still distinguishable right at the start of the reaction (spectrum with triangles up) although relatively smaller than the neighboring peaks. This suggests a rapid reaction between the succinimidyl ester and the IBP (with amide as a product). Toward the end of the reaction (triangle down), the ester peak further decreases due to the reaction progression. No reaction-related amide peak increase is detected since the incremental addition of amide groups during the reaction in an amide-rich solution (from the protein and the Mal-PEG₁₂-NHS) is not easily detected by FTIR.

To obtain IBP-grafted surfaces, the AA2024-SH samples are immersed in different Mal-PEG_{2/12/24}-NH-IBP solutions. The use of solutions with different IBP concentrations and PEG linker lengths led to a range of protein-rich surfaces. Protein enrichment of the surfaces was confirmed by FTIR through the appearance of two protein distinct peaks [28] at 1642 cm⁻¹ (amide I) and 1532 cm⁻¹ (amide II) as seen in Fig. 2d for the modification of the surface with solution 1 from Table 1 as an example.

3.2. Influence of protein degrees of freedom on freezing onset and propagation in the presence of molecular water layer

In natural environments, AFPs are typically found in a liquid medium while INPs are integrated in the bacterial membrane [9,29,30]. Previous research on AFPs in liquids, showed that the ice-suppressing behavior increases initially with the AFP concentration and plateaus when reaching an AFP-dependent specific concentration [19]. To investigate the so far unexplored effect of the AFP concentration on surfaces on frost formation, the AA2024-SH surfaces were immersed in IBP solutions containing Mal-PEG₁₂-NH-AFP and Mal-PEG₁₂-NH-INP at two concentrations (2.5 and 5 mg ml⁻¹) as shown in solutions 1, 2, 5, and 6 in Table 1. The freezing process was followed using a high-resolution thermal camera as explained in the experimental section. Fig. 3a, shows a thermal video snapshot of the local temperature increase due to the latent heat release during freezing. The freezing event here can be seen as a yellow-colored (higher temperature) curved freezing front propagating on the purple-colored (lower temperature) surface as

indicated by the white dashed line and arrows. From these thermal videos (Movies S1-S5), a local temperature at the surface can be obtained and plotted as a function of the time. This allows extracting quantifiable freezing parameters such as freezing onset time (t_{fo}) and temperature (T_{fo}) as shown in Fig. 3b

Fig. 4 shows the values of t_{fo} and T_{fo} of the different AFP-rich samples varying IBP type, IBP concentration and linker length, and the thiol-terminated surface (AA2024-SH) used as reference. Fig. 4a shows how the surfaces coated with anti-freeze proteins (AFP) and ice nucleating proteins (INP) present shorter times to freeze (lower t_{fo}) and more positive temperatures (higher T_{fo}) than the thiol-terminated reference sample (AA2024-SH). INP samples show the expected behavior in line with the ice-nucleating character of INPs. This ice-promoting effect appears to be independent of the INP concentration for the studied concentration range. More unexpected is the behavior of the samples with AFPs. For these samples, t_{fo} decreases and T_{fo} increases with increasing AFP concentration (i.e., freezing happens earlier and at more positive temperatures when more AFP is present at the surface). This trend is opposite to the behaviors reported for AFPs in liquid environments, where higher protein concentrations lead to lower freezing temperatures [19].

The somewhat unexpected results for the AFPs on the surface behaving like the INPs may be explained by the working principle of these proteins in their natural environments and their physical similarities and differences. While INPs typically have molecular weights ranging between 110–130 kDa, the AFPs are typically smaller with molecular weights in the range 2–50 kDa [31,32]. Both types of IBPs have two distinct structural regions: the ice-binding site (IBS) and the non-ice-binding site (NIBS). These regions lead to different water adsorption and structure: adsorbed ordered water molecules at the IBS lead to organized ice-like (INPs) or semicathrate-like (AFP type III) configurations while the water layer on top of the NIBS remains disordered liquid-like when freezing [9,19,33–37]. In other words, surface disorder of the adsorbed water molecules leads to limited or no local ice growth.

As shown in Fig. 5a, INPs in their natural environment generally appear attached to the bacterial membrane with their IBS pointing towards the external water phase. The IBS of the INPs orders water molecules into an ice-like arrangement, which facilitates the kinetically hindered phase transition from liquid water to ice [9,36,37]. Consequently, INPs promote ice formation around the bacterial membrane. This effect is also reflected in the freezing results in Fig. 4a. Furthermore, since INPs are considerably large proteins with large IBSSs, the surface exposed to Mal-PEG₁₂-NH-INP is likely to become rapidly saturated

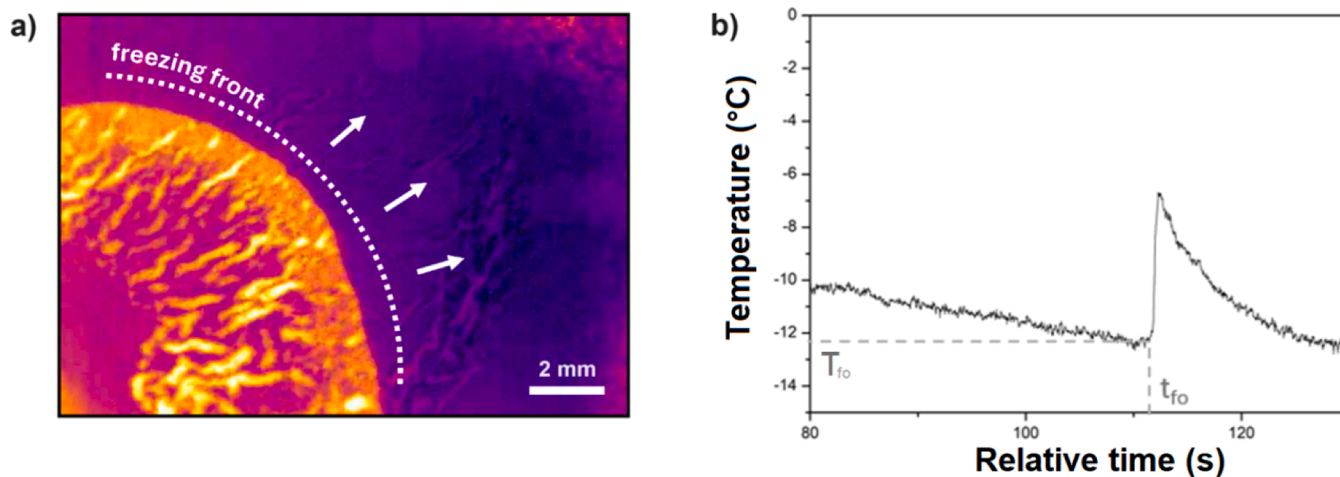


Fig. 3. a) Snapshot from a thermal video showing the freezing-related high-temperature region (yellow) and the progressing freezing front (marked by a dashed white line and arrows) for an IBP-modified aluminum surface. b) Example of time-temperature graph extracted from the thermal video used to determine freezing onset parameters t_{fo} and T_{fo} .

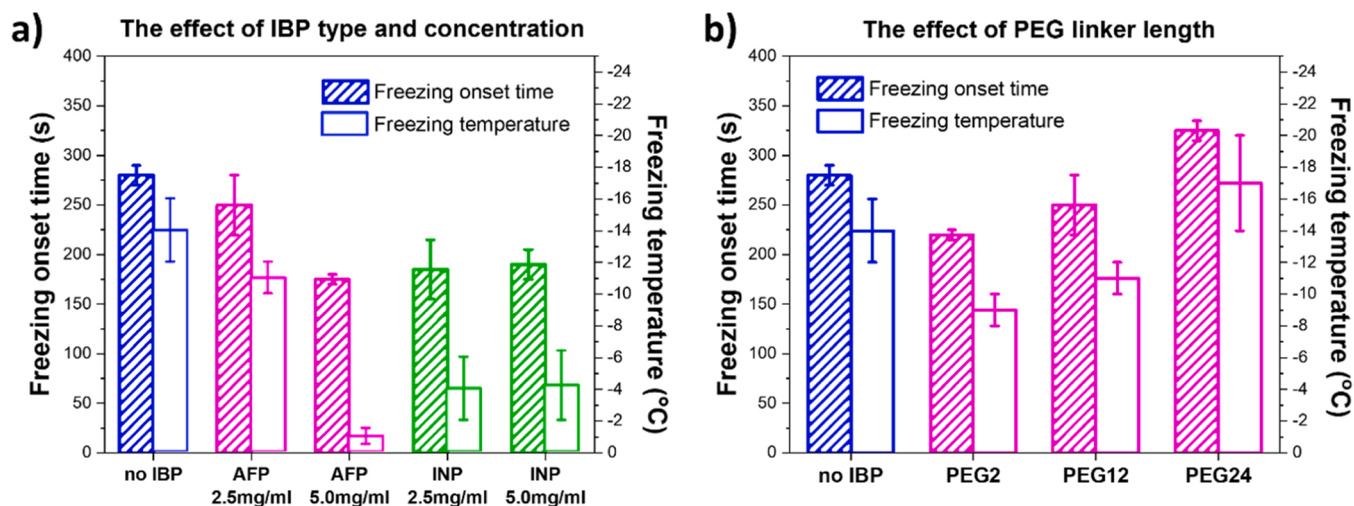


Fig. 4. Freezing onset time (t_{fo}) and freezing temperature (T_{fo}) for different samples: a) t_{fo} and T_{fo} of AA2024-SH before protein grafting (no IBP, blue color), grafted with Mal-PEG₁₂-NH-AFP (magenta color), and grafted with Mal-PEG₁₂-NH-INP (green color) obtained from solutions at two concentrations (2.5 mg ml⁻¹ and 5.0 mg ml⁻¹). b) t_{fo} and T_{fo} of AA2024-SH (no IBP, blue color) and AFP-modified surfaces (magenta color) with various linker lengths (PEG2, PEG12, PEG24).

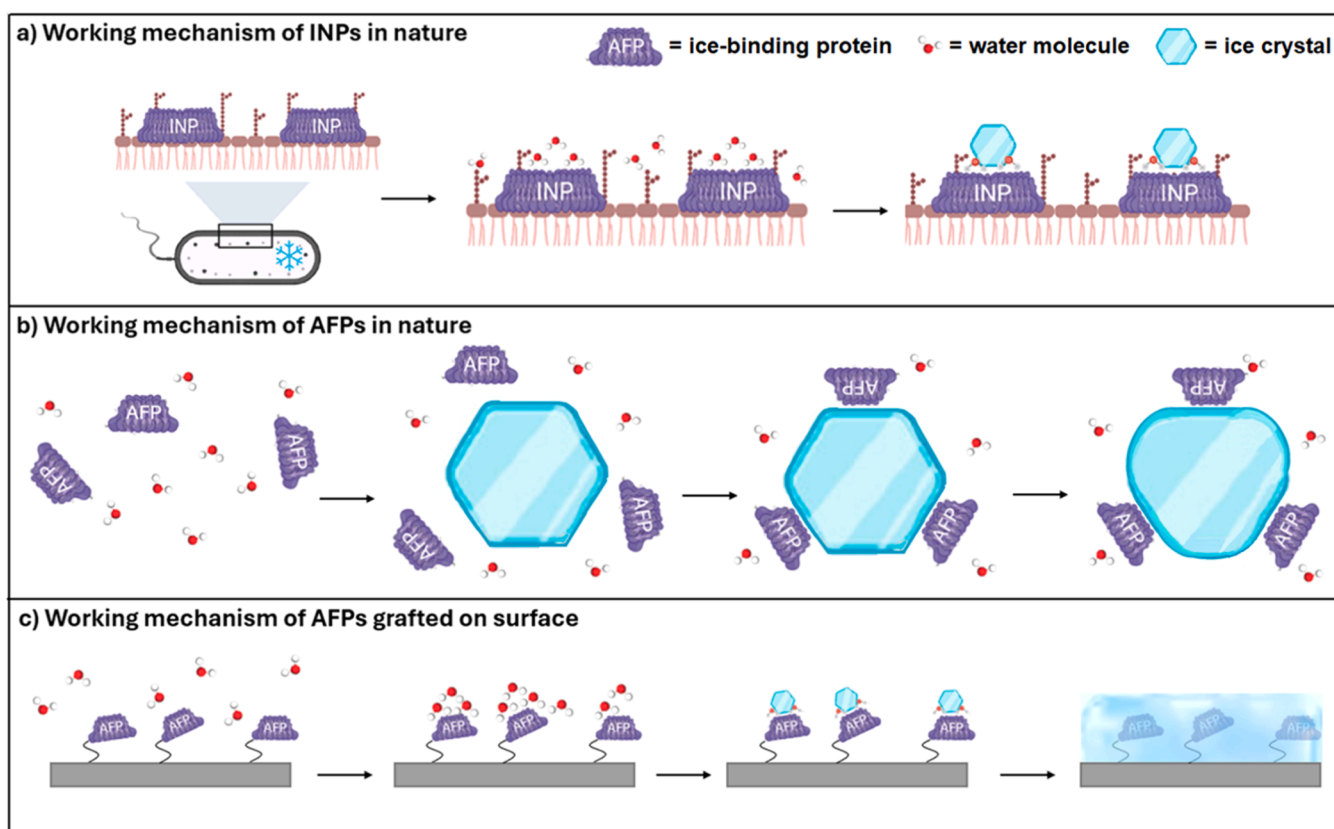


Fig. 5. Illustrations of the working mechanisms of: a) INPs in their natural environment (e.g., present at the exopolymer substances of bacteria) leading to ice nucleation at the surface; b) AFPs in their natural environment (e.g., dispersed in body fluids of fish) leading to ice nucleation surrounded by proteins from their IBS and protected from further growth through their NIBS facing the fluid and the curvature of the trapped ice crystal; and, c) the AFPs grafted on to surfaces as studied in this work leading to ice nucleation and growth due to reduced mobility at the studied concentration and chain length (12 repeated units).

with proteins with IBS at the surface. We therefore hypothesize that the surface saturation was achieved already at 2.5 mg ml⁻¹, hence leading to no measurable effect in the freezing time and temperature when solutions at higher concentrations were used (Fig. 4a).

Unlike INPs, AFPs are generally found in natural fluids rather than surfaces and lead to a somewhat more complex mechanism depicted in Fig. 5b Here, when an ice crystal nucleates in the fluid, the AFPs adsorb

onto the ice crystal using their IBS. Further ice lattice growth at these attachment locations is hence inhibited while being surrounded by the NIBS of the proteins to further limit ice growth. The areas of the ice crystal not covered by proteins keep increasing. This leads to a curvature increase, which in turn increases the free energy of the ice phase to make it energetically unfavorable for water to transition from the liquid to the solid phase and hence further delays ice growth [19].

The results depicted in Fig. 4a for the AFPs do not show this ice-delaying effect. Instead, they show an ice-promoting effect similar to that of the INPs. We attribute this to two factors: (i) the exposed ice-binding site (IBS) of the AFPs promoting ordering of water molecules on the surface, and (ii) the lack of degrees of freedom of the proteins attached to the surface. We argue that these two factors should lead to faster freezing at higher protein concentrations due to a steric effect.

In their natural setting, AFPs can move around and adhere to small ice crystals through their IBS, hence limiting ice growth. We hypothesize that when the AFPs are attached to the surface (at the concentrations and linker length reported in Fig. 4a), their mobility is hindered significantly (as represented in Fig. 5c), thus changing their natural working mechanism. Mobility decrease prohibits the formation of a curved ice front (i.e., bending of the grafted proteins around ice crystals is not possible). As a consequence, the exposed IBSs act as individual templates for ice-like structure nucleation and growth, hence exerting the opposite of the intended effect (i.e., AFPs grafted on surfaces behave as INPs in Fig. 5a). By increasing the AFP concentration on the surface, the number of IBSs increases, further enhancing their ice-promoting effect (Fig. 5c) as observed in Fig. 4a at higher AFP concentrations.

It is also important to note that the grafting approach chosen in this work targets the N-terminus of each IBP, thus ensuring that the IBSs of the type III AFPs are fully exposed to the surface. On the other hand, the INP is a β -helical protein with its end groups located at both bases of the cylindrical structure [31,32]. Therefore, the IBSs and NIBSs of the INPs are equally exposed after the surface grafting, which likely reduces the efficiency of their ice-nucleating function shown in Fig. 4. The IBSs on samples grafted with AFPs are perfectly exposed for maximum binding to ice, whereas on samples grafted with INPs, the IBSs are less ideally oriented on the surface, thus resulting in less efficient ice growth promotion than expected for INPs.

To further demonstrate our hypothesis that protein mobility and degrees of freedom from an anchored point at a surface is a crucial factor in the (anti)freezing character of (grafted) AFPs, we synthesized the same AFP but with different linker lengths and grafted them on AA2024-SH using solutions 1, 3, 4 shown in Table 1. Fig. 4b shows the effect of

the linker length on T_{f0} and t_{f0} . The results show how increasing the linker length (from PEG2 to PEG24) leads to longer times to freeze (t_{f0}) and more negative freezing temperatures (T_{f0} depletion) outperforming the values for the reference hydrophilic silanized sample (AA2024-SH). In line with this idea, if the increasing PEG linker length would lead to lower grafting density due to steric effects reducing reactivity of the grafting, the results would have been opposite (i.e., showing a higher ice-promoting effect with the long PEG-24 linker). This result is compatible with our hypothesis that protein mobility induced by flexible long chain linkers leads to higher anti-freezing character. We further argue that this mobility increase is partly possible due to the presence of a molecular water layer (MWL) formed by the hydrophilic character of AFPs, as supported by the low WCAs < 20° of these samples (Fig. 2a).

A close analysis of the freezing front mode and kinetics (Fig. 6 and Movies S1-S2 in the support information) confirms the freezing kinetics of protein-rich surfaces to be in the range of 40–70 mm s⁻¹ with no clear PEG-length dependency and with a smooth (non-fractal) frontline compatible with the values and propagation frontline mode reported for frost freezing on hydrophilic surfaces with MWLs [30]. Freezing on the AA2024-SH surfaces shows, on the other hand, a fractal frontline and propagation and much slower propagation rates (around 0.2 mm s⁻¹). This further confirms that the grafted PEG-AFPs increase hydrophilicity of the surface making MWLs more continuous, as illustrated in Fig. 6. The results suggest that the AFP's ability to promote the formation of MWLs accelerates freezing propagation rates and raises the temperature at which freezing onset occurs (Fig. 4a). Nevertheless, freezing at the surface is counteracted when the proteins have sufficient degrees of freedom in the MWL as achieved by longer linker length and experimentally observed by a depression of the freezing temperature below that of the reference sample and longer freezing onset times (Fig. 4b). In other words, the data supports our hypothesis that AFPs recover the ice-depressing function they show in their natural environment when they get sufficient degrees of freedom in a water-rich layer (MWL), a factor that should be considered in future anti-freezing surface developments using IBPs.

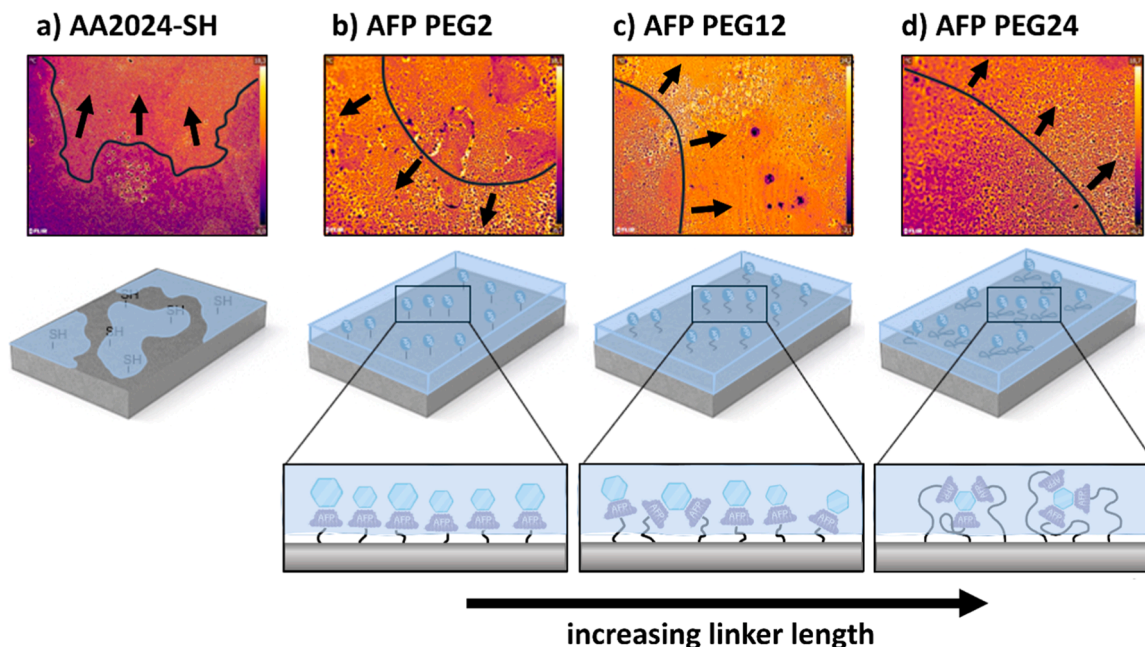


Fig. 6. Freezing front propagation on AA2024-SH (propagation rate of 0.2 ± 0.08 mm s⁻¹) and on surfaces with AFPs grafted using PEG2, PEG12, and PEG24 linker lengths (propagation rates between 40–70 mm s⁻¹). The high propagation speeds on the AFP surfaces confirm the presence of continuous MWLs on these samples (MWL represented here with a blue box). It is hypothesized that, at sufficiently high linker lengths, the AFPs regain their ice-depressing character due to increased mobility as observed by a drop in T_{f0} and t_{f0} . For the higher linker lengths, this mobility, in combination with the continuous MWL at the IBPs away from the metal surface, makes it possible for the AFPs to gain degrees of freedom and act in a similar way as they would in their natural environment to inhibit ice growth.

3.3. AFP-induced freezing delay in confined polymeric environments rich in water

To further investigate the role of the environment, water layers, and degrees of freedom on the anti-freezing character of AFPs and approximate their potential use in organic coatings, hydrogels grafted with IBPs were synthesized as shown in the experimental section. Due to the rapid gelation of the hydrogel used in this work, a co-injection chamber (CIJ) [21], as illustrated in Fig. 7, was used to directly apply the hydrogels on the AA2024-SH surfaces. In this approach, two separate solutions are simultaneously sprayed onto the substrate after a short residence time in a mixing chamber (Fig. 7).

In our work, one solution contains PEG dithiol in PBS, while a second solution contains a four-arm-PEG-maleimide mixed with maleimide-modified AFPs in PBS with the AFPs at two different concentrations. The two solutions are manually positioned with a syringe into separate chambers of the CIJ and simultaneously pushed at high pressure into the mixing chamber and directly onto the metal surface. The thiol-maleimide click chemistry allowed simultaneously a rapid reaction between the hydrogel and the thiol-rich surface and cross-linking of the hydrogel network. A similar strategy was used to incorporate INPs in the hydrogel. However, due to their large size, the INPs are expected to be physically trapped in the hydrogel network instead of covalently bonded to the polymer backbone of the hydrogel as happens for the AFPs.

Fig. 8a shows the freezing onset temperature (T_{fo}) and onset time (t_{fo}) for the different hydrogels. As expected, the presence of INPs in the hydrogels induces freezing at more positive temperatures (T_{fo}) and accelerates freezing (lower t_{fo}) with respect to the reference hydrogel

without IBPs. This effect is slightly more pronounced when more INPs are used (2.5 mg ml^{-1} vs 5.0 mg ml^{-1}). Contrary to this effect, hydrogels containing AFPs have longer t_{fo} (freezing happens later) and a more negative T_{fo} when the AFP concentration increases. This confirms that the AFPs grafted inside a hydrated hydrogel network can successfully delay ice growth despite their hydrophilic character.

In agreement with the effects observed when grafted on surfaces using long dangling chains in the presence of a molecular water layer, we attribute the positive effect of AFPs in a hydrated hydrogel with low crosslinking density to the relatively high mobility induced by several factors increasing AFP degrees of freedom in a theoretically constrained media: (i) most AFPs in the hydrogel are attached to one arm of the 4-arm-PEG-maleimide (dark blue line) through a PEG dithiol molecule (red line) (i.e., dangling arms) as represented in Fig. 7; (ii) in such an environment, the water acts as a solubilizing medium protecting the AFPs from denaturation and ensuring their optimal function through mobility; and (iii) the hydrophilic character of PEG chains, allows the formation of a hydration layer adsorbed through hydrogen bonding (represented in Fig. 7 as dark blue area around the red chains) that prevents protein adsorption on the polymer backbone as observed in protein resistant polymers [38].

To further confirm our hypothesis proposing that the degrees-of-freedom of physically connected AFPs to polymers and surfaces is a key factor in controlling ice growth and propagation using AFPs, the hydrogels were dehydrated and subjected again to the same freezing tests. Fig. 8b shows the corresponding freezing results. For hydrogels without IBPs, dehydration (Fig. 8b) leads to freezing at much longer times (450 s vs 150 s) and lower temperatures (-21°C vs -11.5°C) than

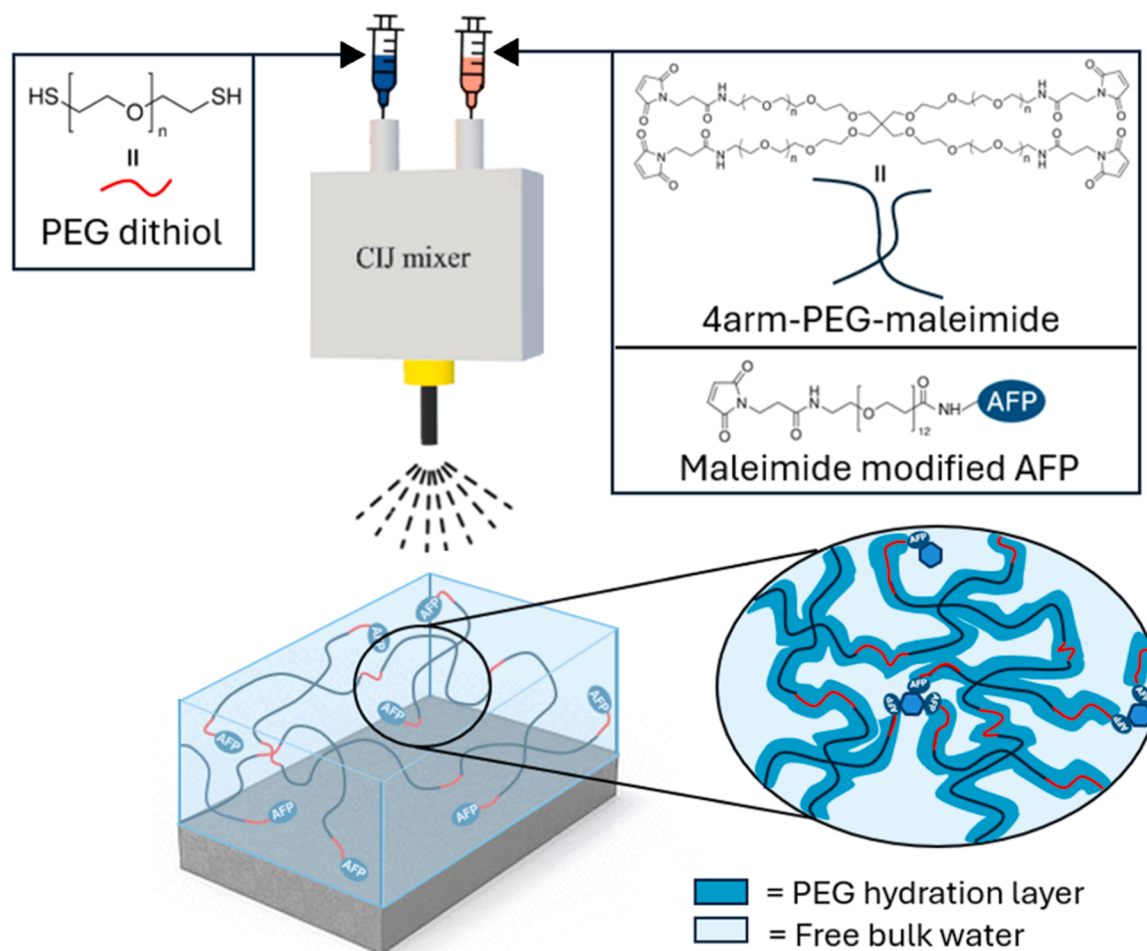


Fig. 7. Rapid deposition of $500 \mu\text{m}$ -thick hydrogels onto AA2024-SH substrate using a co-injection mixer (CIJ). The long PEG linker length and hydration layer within the resulting hydrogel ensure high AFP mobility and functioning (bottom right image).

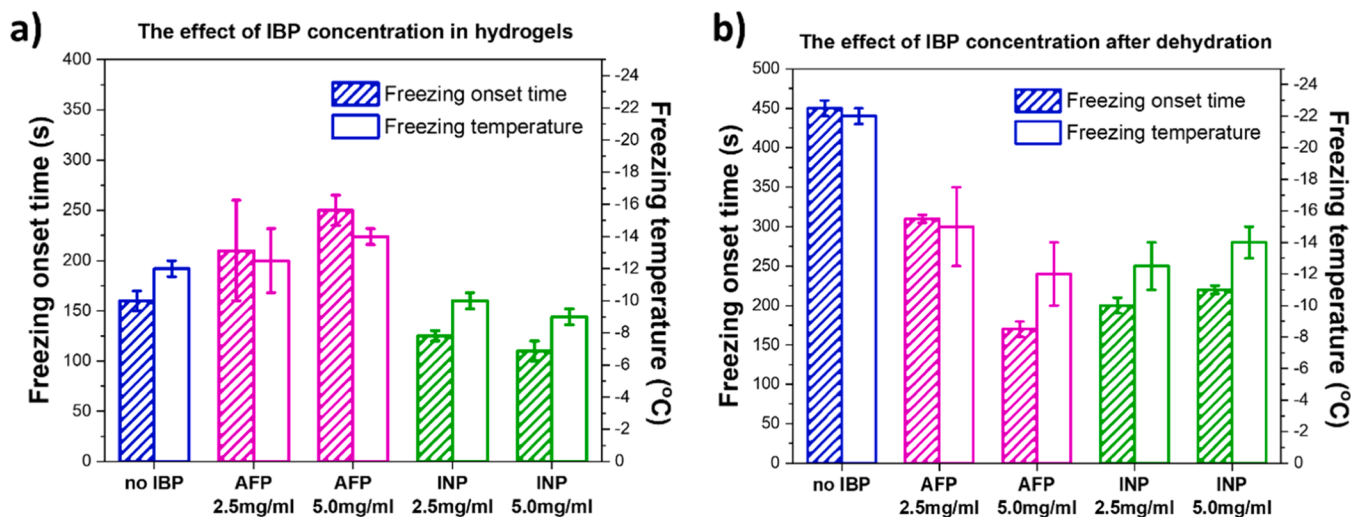


Fig. 8. a) t_{f0} and T_{f0} of the hydrogels with no IBPs (blue color), with AFPs (magenta color), and with INPs (green color) at two concentrations (2.5 mg ml^{-1} and 5.0 mg ml^{-1}). b) t_{f0} and T_{f0} of the dehydrated hydrogels with no IBPs (blue color), with AFPs (magenta color), and with INPs (green color) at two concentrations (2.5 mg ml^{-1} and 5.0 mg ml^{-1}).

the hydrated hydrogels (Fig. 8a). Such an effect might be attributed to the balance between *freezable* and *non-freezable water* content as recently demonstrated in ionic polymers [22,39]. Freezable water is further subdivided into *freezable free water* and *freezable bound water*, depending on the interactions between the water and the polymer network. *Freezable free water* has no interactions with the polymer structure while *freezable bound water* has limited interactions with the polymer structure (adsorbed water). We hypothesize that these interactions slow down the reorientation of water into an ice-like lattice, thus retarding ice growth. On the other hand, non-freezing water is tightly bound to the flexible polymeric structure (adsorbed water), preventing these water molecules from orienting into an ice-like lattice and thereby preventing freezing [22,39].

The amount of these three different types of water in the hydrogel systems with different AFP concentrations was analyzed in this study using differential scanning calorimetry (DSC) following the guidelines reported in a recent study [22]. As seen in Fig. 9, the amount of freezable free water decreases when the AFPs are present in the hydrogel, while simultaneously, the amount of non-freezing water increases. Even though there are no significant changes between the two AFP concentrations, the increase in non-freezing water and decrease of freezable free water in the AFP-hydrogels supports the conclusion that the AFPs grafted inside a hydrated hydrogel network successfully inhibit ice growth (Fig. 8a). Moreover, recent findings studying hydrogels with various levels of hydration show how drying reduces the amount of freezable free water until only non-freezing water remains [40].

Following this reasoning, the large differences in freezing data between dehydrated and hydrated hydrogels can be explained. The hydrated hydrogels contain freezable free, freezable bound, and non-freezing water. The freezable free water freezes quickly as captured by the thermal camera (Movies S3 and S4). On the other hand, the dehydrated hydrogels will likely only contain non-freezing and freezable bound water. Since freezable bound water reorients itself at a slower rate compared to freezable free water the dehydrated hydrogels freeze at a slower freezing propagation rate as detected by thermal imaging (Movie S5).

Conversely, the presence of AFP and INPs in a dry hydrogel accelerates freezing at more positive temperatures (Fig. 8b) with no significant differences between IBP type and concentration. This result is compatible with the hypothesis of the mobility discussed in this work, as lack of mobility in IBPs (INP and AFP) magnifies the ice acceleration effect of proteins with ice-binding sites (IBS) to further prove that

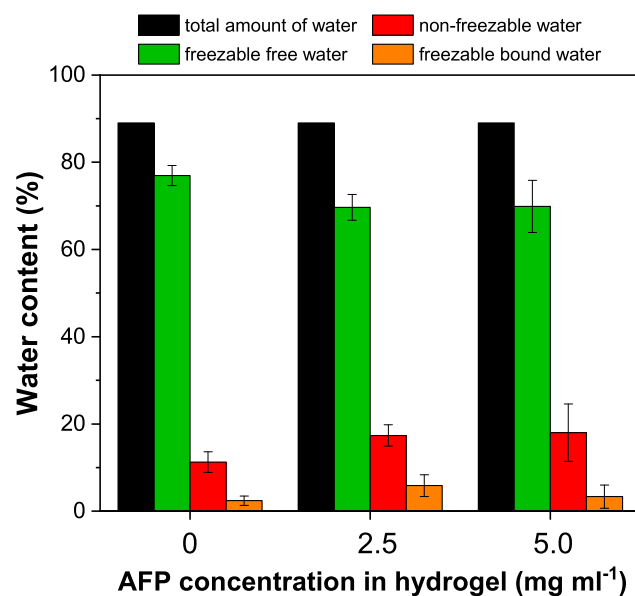


Fig. 9. The amount of freezable free (green), freezable bound (orange), and non-freezable (red) water in the hydrogel systems with different AFP concentrations. The amount of freezable free water decreases when the AFPs are introduced into the hydrogel, while simultaneously, the amount of non-freezing water slightly increases.

protein mobility is crucial to obtain ice delaying effects when using antifreeze proteins.

Overall, these findings demonstrate that while AFPs can be useful in delaying ice formation, their successful use heavily depends on maintaining an environment that provides sufficient degrees of freedom for the proteins. As summarized in Fig. 10, increasing the PEG linker length of the grafted AFPs or maintaining a hydration layer for AFPs in hydrogel matrices will ensure that the proteins have sufficient mobility to inhibit ice crystal growth on surfaces.

4. Conclusions

Two different types of IBPs (AFP and INP) were covalently attached to aluminum alloy (AA2024) surfaces and to the polymer backbone of a

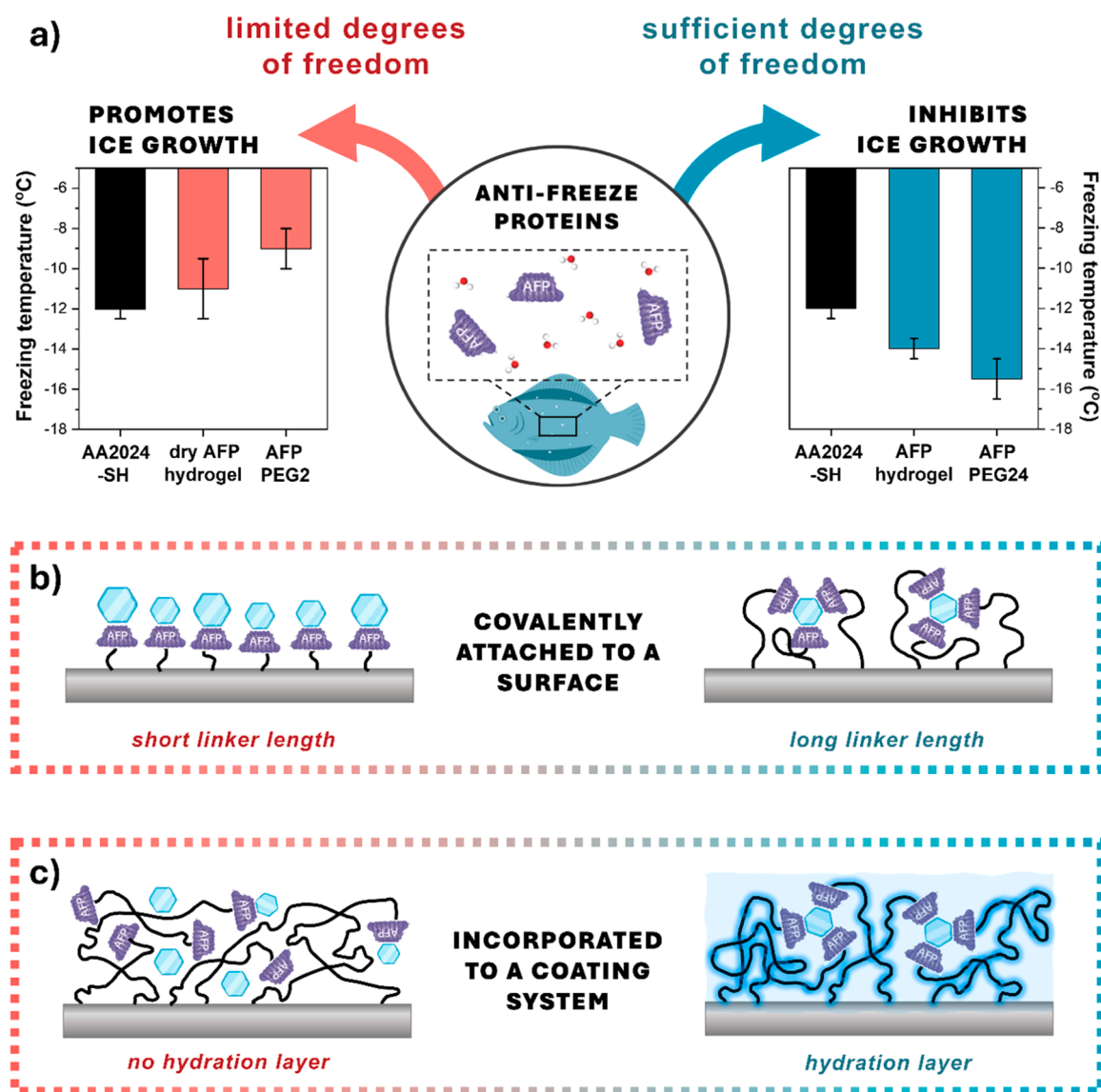


Fig. 10. a) The AFPs are found to promote ice growth if they are incorporated on surfaces with limited degrees of freedom (left side). With sufficient degrees of freedom, the AFPs can inhibit ice growth on surfaces by lowering the freezing onset temperature and time (right side). b) AFPs covalently linked to surfaces require long chain lengths to provide sufficient degrees of freedom in the presence of molecular water layers, whereas c) inside a polymer network, a hydration layer is needed to ensure AFP mobility.

hydrogel using different linker chain lengths and protein concentrations. The results confirm the ice-promoting effect of INPs in all cases independently of the INP concentration used. AFPs, on the other hand, show a large dependency on the dangling chain length and protein concentration when grafted on surfaces or dangled in a PEG polymer backbone. The systematic study demonstrates the relevance of AFP mobility (degrees of freedom) in the reduction of ice accretion when grafting AFPs with their IBs exposed to the solution. While AFPs lead to the formation of molecular water layers (MWL) due to the overall hydrophilic character of the PEG-AFPs, long dangling chains enhance protein degrees of freedom in the MWL to prevent ice propagation. Conversely, in a constrained environment as a polymer hydrogel, hydration is responsible for the mobility of the dangling proteins and the related drop in freezing temperature and increase in freezing onset time. The findings here reported unveil a new design factor using AFPs and clear the path to the effective use of natural or synthetic AFPs in cutting-edge domains such as surfaces for (long-term) cryopreservation of biological samples, food preservation, electronics and sensors, and the creation of next-generation bioinspired low-icing functional coatings for wind-turbines

and aircraft.

CRediT authorship contribution statement

Laura Hoebus: Writing – original draft, Visualization, Investigation, Formal analysis, Data curation. **Miisa J. Tavaststjerna:** Writing – review & editing, Visualization, Supervision, Methodology, Investigation, Formal analysis, Data curation, Conceptualization. **Santiago J. Garcia:** Writing – review & editing, Visualization, Validation, Supervision, Methodology, Funding acquisition, Formal analysis, Conceptualization.

Declaration of competing interest

The authors declare that they have no known competing financial interests or personal relationships that could have appeared to influence the work reported in this paper.

Acknowledgments

This project has received funding from the European Union's Horizon 2020 research programme under the Marie Skłodowska-Curie grant agreement No 956703 (SURFICE project).

Supplementary materials

Supplementary material associated with this article can be found, in the online version, at [doi:10.1016/j.apsadv.2025.100790](https://doi.org/10.1016/j.apsadv.2025.100790).

Data availability

Data will be made available on request.

References

- H. He, Z. Guo, Superhydrophobic materials used for anti-icing: theory, application, and development, *iScience* 24 (2021) 103357, <https://doi.org/10.1016/j.isci.2021.103357>.
- A.A. Yancheshme, A. Allahdini, K. Maghsoudi, R. Jafari, G. Momen, Potential anti-icing applications of encapsulated phase change material-embedded coatings; a review, *J. Energy Storage* 31 (2020) 101638, <https://doi.org/10.1016/j.est.2020.101638>.
- J.L. Laforte, M.A. Allaire, J. Laflamme, State-of-the-art on power line de-icing, *Atmos. Res.* 46 (1998) 143–158, [https://doi.org/10.1016/S0169-8095\(97\)00057-4](https://doi.org/10.1016/S0169-8095(97)00057-4).
- K. Wei, Y. Yang, H. Zuo, D. Zhong, A review on ice detection technology and ice elimination technology for wind turbine, *Wind Energy* 23 (2020) 433–457, <https://doi.org/10.1002/we.2427>.
- Y. Cao, W. Tan, Z. Wu, Aircraft icing: an ongoing threat to aviation safety, *Aerosp. Sci. Technol.* 75 (2018) 353–385, <https://doi.org/10.1016/j.ast.2017.12.028>.
- S.S. Lathje, R.S. Sutar, A.K. Bhosale, S. Nagappan, C.-S. Ha, K.K. Sadasivuni, S. Liu, R. Xing, Recent developments in air-trapped superhydrophobic and liquid-infused slippery surfaces for anti-icing application, *Prog. Org. Coat.* 137 (2019) 105373, <https://doi.org/10.1016/j.porgcoat.2019.105373>.
- R. Suris-Valls, I.K. Voets, Peptidic antifreeze materials: prospects and challenges, *Int. J. Mol. Sci.* 20 (2019) 5149, <https://doi.org/10.3390/ijms20205149>.
- A. Ampaw, T.A. Charlton, J.G. Briard, R.N. Ben, Designing the next generation of cryoprotectants – From proteins to small molecules, *Pept. Sci.* 111 (2018) e24086, <https://doi.org/10.1002/pep2.24086>.
- A. Eskandari, T.C. Leow, M.B.A. Rahman, S.N. Oslan, Antifreeze proteins and their practical utilization in industry, *Med. Agric., Biomol.* 10 (2020) 1649, <https://doi.org/10.3390/biom10121649>.
- M. Lukas, R. Schwidetzky, R. Eufemio, M. Bonn, K. Meister, Toward understanding bacterial ice nucleation, *J. Phys. Chem. B* 126 (2022) 1861–1867, <https://doi.org/10.1021/acs.jpcc.1c09342>.
- Z.F. Brotzakis, M. Gehre, I.K. Voets, P.G. Bolhuis, Stability and growth mechanism of self-assembling putative antifreeze cyclic peptides, *Phys. Chem. Chem. Phys.* 19 (2017) 19032, <https://doi.org/10.1039/C7CP02465G>.
- I.K. Voets, From ice-binding proteins to bio-inspired antifreeze materials, *Soft Matter* 13 (2017) 4808–4823, <https://doi.org/10.1039/C6SM02867E>.
- R.P. Tas, V. Sampaio-Pinto, T. Wennekes, L.W. van Laake, I.K. Voets, From the freezer to the clinic, *EMBO Rep.* 22 (2021) e52162, <https://doi.org/10.15252/embr.202052162>.
- Y. Gwak, J.-I. Park, M. Kim, H. Kim, M. Kwon, S. Oh, Y.-P. Kim, E. Jin, Creating anti-icing surfaces via the direct immobilization of antifreeze proteins on aluminum, *Sci. Rep.* 5 (2015) 12019, <https://doi.org/10.1038/srep12019>.
- A. Esser-Kahn, V. Trang, M. Francis, Incorporation of antifreeze proteins into polymer coatings using site-selective bioconjugation, *J. Am. Chem. Soc.* 132 (2010) 13264, <https://doi.org/10.1021/ja103038p>.
- T. Charpentier, A. Neville, P. Millner, R. Hewson, A. Morina, An investigation of freezing of supercooled water on anti-freeze protein modified surfaces, *J. Bionic Eng.* 10 (2013) 139–147, [https://doi.org/10.1016/S1672-6529\(13\)60208-5](https://doi.org/10.1016/S1672-6529(13)60208-5).
- Y. Jeong, S. Jeong, Y.K. Nam, S.M. Kang, Development of freeze-resistant aluminum surfaces by tannic acid coating and subsequent immobilization of antifreeze proteins, *Bull. Korean Chem. Soc.* 39 (2018) 559–562, <https://doi.org/10.1002/bkcs.11406>.
- Y. Gao, H. Qi, D. Fan, J. Yang, L. Zhang, Beetle and mussel-inspired chimeric protein for fabricating anti-icing coating, *Colloids Surf. B: Biointerfaces* 210 (2022) 112252, <https://doi.org/10.1016/j.colsurfb.2021.112252>.
- E. Kristiansen, K.E. Zachariassen, The mechanism by which fish antifreeze proteins cause thermal hysteresis, *Cryobiology* 51 (2005) 262–280, <https://doi.org/10.1016/j.cryobiol.2005.07.007>.
- K. Liu, C. Wang, J. Ma, G. Shi, X. Yao, H. Fang, Y. Song, J. Wang, Janus effect of antifreeze proteins on ice nucleation, *Proc. Natl. Acad. Sci.* 113 (2016) 14739, <https://doi.org/10.1073/pnas.1614379114>.
- J. Han, Z. Zhu, H. Qian, A.R. Wohl, C.J. Beaman, T.R. Hoye, C.W. Macosko, Simple confined impingement jets mixer for flash nanoprecipitation, *J. Pharm. Sci.* 101 (2012) 4018–4023, <https://doi.org/10.1002/jps.23259>.
- R.A. Biro, E.C. Tyrode, E. Thormann, Reducing ice adhesion to polyelectrolyte surfaces by counterion-mediated nonfrozen hydration water, *ACS Appl. Mater. Interfaces* 16 (2024) 21356, <https://doi.org/10.1021/acsmi.4c02434>.
- M.J. Tavaststjerna, S.J. Picken, S.J. Garcia, Role of molecular water layer State on freezing front propagation rate and mode studied with thermal imaging, *Langmuir* 40 (2024) 12888, <https://doi.org/10.1021/acs.langmuir.4c00323>.
- J. Sieber, J. Ducke, A. Rietig, T. Langner, J. Acker, Recovery of Li (Ni_{0.33}Mn_{0.33}Co_{0.33})O₂ from lithium-ion battery cathodes: aspects of degradation, *Nanomaterials* 9 (2019) 246, <https://doi.org/10.3390/nano9020246>.
- M. Taghavikish, S. Subianto, N. Dutta, N.R. Choudhury, Novel thiol-ene hybrid coating for metal protection, *Coatings* 6 (2016) 17, <https://doi.org/10.3390/coatings6020017>.
- D. Tsiourvas, A. Tsetsekou, M. Arkas, S. Diplas, E. Mastrogianni, Covalent attachment of a bioactive hyperbranched polymeric layer to titanium surface for the biomimetic growth of calcium phosphates, *J. Mater. Sci.: Mater. Med.* 22 (2011) 85–96, <https://doi.org/10.1007/s10856-010-4181-7>.
- T. Oh, Comparison between SiOC thin film by plasma enhance chemical vapor deposition and SiO₂ thin film by fourier transform infrared spectroscopy, *J. Korean Phys. Soc.* 56 (2010) 1150–1155, <https://doi.org/10.3938/jkps.56.1150>.
- L.M. Miller, M.W. Bourassa, R.J. Smith, FTIR spectroscopic imaging of protein aggregation in living cells, *Biochim. Biophys. Acta (BBA) - Biomembr.* 1828 (2013) 2339–2346, <https://doi.org/10.1016/j.bbame.2013.01.014>.
- M. Bar Dolev, I. Braslavsky, P.L. Davies, Ice-binding proteins and their function, *Annu. Rev. Biochem.* 85 (2016) 515–542, <https://doi.org/10.1146/annurev-biochem-060815-014546>.
- A. Bialkowska, E. Majewska, A. Olezak, A. Twarda-Clapa, Ice binding proteins: diverse biological roles and applications in different types of industry, *Biomolecules* 10 (2020) 274, <https://doi.org/10.1016/j.jbiomac.2021.08.105>.
- A. Baskaran, M. Kaari, G. Venugopal, R. Manikkam, J. Joseph, P.V. Bhaskar, Anti freeze proteins (Afp): properties, sources and applications – A review, *Int. J. Biol. Macromol.* 189 (2021) 292–305, <https://doi.org/10.1016/j.jbiomac.2021.08.105>.
- S. Hartmann, M. Ling, L.S.A. Dreyer, A. Zipori, K. Finster, S. Grawe, L.Z. Jensen, S. Borck, N. Reicher, T. Drace, D. Niedermeier, N.C. Jones, S.V. Hoffmann, H. Wex, Y. Rudich, T. Boesen, T. Santl-Temkiv, Structure and protein-protein interactions of ice nucleation proteins drive their activity, *Front. Microbiol.* 13 (2022) 872306, <https://doi.org/10.3389/fmicb.2022.872306>.
- K. Mochizuki, V. Molinero, Antifreeze glycoproteins bind reversibly to ice via hydrophobic groups, *J. Am. Chem. Soc.* 140 (2018) 4803–4811, <https://doi.org/10.1021/jacs.7b13630>.
- P. Pal, S. Chakraborty, B. Jana, Deciphering the role of the non-ice-binding surface in the antifreeze activity of hyperactive antifreeze proteins, *J. Phys. Chem. B* 124 (2020) 4686–4696, <https://doi.org/10.1021/acs.jpcc.0c01206>.
- P. Pal, S. Chakraborty, B. Jana, Differential hydration of ice-binding surface of globular and hyperactive antifreeze proteins, *Adv. Theory Simul.* 4 (2021) 2100090, <https://doi.org/10.1002/adts.202100090>.
- R. Aich, P. Pal, S. Chakraborty, B. Jana, Preferential ordering and organization of hydration water favor nucleation of ice by ice-nucleating proteins over antifreeze proteins, *J. Phys. Chem. B* 127 (2023) 6038–6048, <https://doi.org/10.1021/acs.jpcc.3c01641>.
- P. Pal, S. Chakraborty, B. Jana, Molecular insight of the ice nucleation by ice binding protein: a comparative study with ice nucleating protein, antifreeze protein, and non-ice-binding protein, *J. Phys. Chem. C* 129 (2025) 600–610, <https://doi.org/10.1021/acs.jpcc.4c05443>.
- B.K.D. Ngo, M.A. Grunlan, Protein resistant polymeric biomaterials, *ACS Macro Lett.* 6 (2017) 992–1000, <https://doi.org/10.1021/acsmacrolett.7b00448>.
- E. Lee, J. Lee, D. Kim, K. Jeong, J.-H. Seo, Investigation of hydration state effects on ice and frost formation on hydrogel-coated surfaces for enhanced anti-icing/frosting properties, *Prog. Org. Coat.* 197 (2024) 108857, <https://doi.org/10.1016/j.porgcoat.2024.108857>.
- J. Ostrowska-Czubenko, M. Pieróg, M. Gierszewska-Drużyńska, Effect of ionic crosslinking on the water state in hydrogel chitosan membranes, *Carbohydr. Polym.* 77 (2009) 590–598, <https://doi.org/10.1016/j.carbpol.2009.01.036>.